

Modelling the Effect of the Exposure to Perfluorooctanoate (PFOA) and Perfluorooctane Sulfonate (PFOS) on Thyroid Homeostasis

CHONTITA RATTANAKUL
Department of Mathematics,
Faculty of Science,
Mahidol University,
Bangkok,
THAILAND

also with
Centre of Excellence in Mathematics,
MHESI,
Bangkok,
THAILAND

Abstract: - Thyroid homeostasis is crucial for the human body. The imbalance of thyroid homeostasis might cause diseases such as hypothyroidism. Humans are exposed to PFOS/PFOA frequently since they have been used in various industrial products. As reported that PFOS/PFOA increase the metabolic clearance rate of thyroid hormones, we then develop a mathematical model in terms of a system of differential equations to investigate thyroid homeostasis based on the changes in the levels of thyrotropin-releasing hormone, thyroid-stimulating hormone and thyroid hormones when the effect of the exposure to PFOS and PFOA is also incorporated as well. The geometric singular perturbation technique is then employed to identify the possible dynamic behaviours obtained from the model. Numerical investigations are also presented to illustrate the results from theoretical analysis. Both theoretical and numerical results imply that a periodic behaviour that has been observed clinically in the pulsatile secretions of thyroid hormones, thyroid-stimulating hormone and thyrotropin-releasing hormone could be obtained from our model. In addition, the numerical experiment also shows that the levels of thyroid hormones and thyroid-stimulating hormone for the case when there is the effect of exposure to PFOS and PFOA are lower than those of the case when there is no effect of the exposure to PFOS and PFOA which might lead to the imbalance of thyroid homeostasis.

Key-Words: - Thyroid hormones, thyrotropin-releasing hormone, thyroid-stimulating hormone, perfluorooctane sulfonate, perfluorooctanoate, mathematical model

Received: November 19, 2022. Revised: July 19, 2023. Accepted: August 17, 2023. Published: September 12, 2023.

1 Introduction

Thyroid hormones (THs) secreted by the follicular cells of the thyroid gland are necessary for the differentiation of cells, and growth, and also regulate significant metabolisms, [1]. The release of thyroid hormones is regulated by the negative feedback control on the hypothalamus and anterior pituitary, [2]. When the circulating levels of thyroid hormones (Triiodothyronine (T3) and Thyroxine (T4)) are low, the secretion of thyrotropin-releasing hormone (TRH) from the hypothalamus will be increased, [2]. Then, the increase in TRH level

stimulates the anterior pituitary gland to produce thyroid-stimulating hormone (TSH). The thyroid gland is then stimulated by the increase of TSH to produce thyroid hormones until levels of thyroid hormones in the blood return to normal levels, [2]. Thyroid homeostasis is crucial for the human body. The imbalance of thyroid homeostasis might cause diseases such as hypothyroidism. Hence, the balance of thyroid homeostasis must be kept.

Perfluorooctane sulfonate (PFOS) and perfluorooctanoate (PFOA) are synthetic compounds in the group of per- and polyfluoroalkyl substances (PFASs) used in many industrial

applications such as firefighting foam, floor wax, paints, food packaging, cookware, cosmetics and textiles for decades, [3], [4]. Humans are exposed to PFAS because they accumulate in soil and waters, persisting for years and are difficult to eliminate, [3]. The contamination of PFASs in surface water, groundwater and soil has been reported frequently, [5], [6], [7]. Therefore, if the use of PFASs is continued, the contamination of PFASs will also continue and accumulate in drinking water, food and the environment which could lead to a global environmental pollutants crisis that could also threaten human health, [5]. Exposure to PFOA is related to the dysfunctions of the thyroid and cancer related to the kidney and testicular, [3]. On the other hand, exposure to PFOS is also related to a decrease in fertility and adverse effects on the development of the fetus, [3]. In children, an impaired immune response is also reported to be related to exposure to PFOS and PFOA whereas increased levels of cholesterol and obesity are also observed in adults, [3]. In this paper, we investigate the effect of exposure to PFOS/PFOA on thyroid homeostasis using mathematical modelling which has never been studied before. As it has been reported in, [8], PFOS and PFOA increase the metabolic clearance rate of thyroid hormones which affects thyroid homeostasis by reducing the circulating levels of thyroid hormones in diet-exposed animals, a system of differential equations is then developed in the next section based upon the changes in the levels of TRH, TSH, THs when the effect of PFOS and PFOA is incorporated.

2 Model Development and Analysis

Here, we let X , Y and Z represent the concentrations of TRH, TSH and THs in blood at time T , respectively. We propose the following mathematical model in terms of a system of differential equations to investigate the effect of PFOS and PFOA on thyroid homeostasis.

$$\frac{dX}{dT} = \frac{a_1}{h_1 + X} + \frac{a_2 XZ}{h_2 + Z^2} - b_1 X \quad (1)$$

$$\frac{dY}{dT} = \frac{a_3 XY(a_4 + a_5 Y)}{(h_3 + X)(h_4 + Z)(h_5 + Y^2)} - a_6 Y - b_2 Y \quad (2)$$

$$\frac{dZ}{dT} = \frac{a_7}{h_6 + Z} + a_8 Y - b_3 Z \quad (3)$$

where we assume the positive values for all parameters in the system of equations (1)-(3).

Equation (1) accounts for the rate of change of TRH's level in blood at time T . The feedback control of TRH on its secretion from the hypothalamus is presented by the first term on the right of (1) while the increase in the secretion of TRH due to the stimulation of THs is presented by the second term and the rate at which TRH is removed from the system is presented by the third term.

Equation (2) accounts for the rate of change of TSH's level in blood at time T . The secretion of TSH from the anterior pituitary gland due to the stimulating effect of TRH, the feedback control of TSH on its secretion from the anterior pituitary gland and the secretion of TSH due to the level of this is presented by the first term on the right of equation (2). The metabolic clearance rate of TSH due to the exposure to PFOS and PFOA is presented in the second term while the rate at which TSH is removed from the system is presented in the third term.

Equation (3) accounts for the rate of change of THs's level in blood at time T . The feedback control of THs on its secretion from the thyroid gland is presented by the first term on the right of equation (3). The secretion of THs from the thyroid gland due to the level of TSH is presented by the second term while the rate at which THs are removed from the system is presented by the third term.

It has been reported that the half-life of TRH and TSH are approximately 6 minutes, [9], and 60 minutes, [10], respectively. The half-life for THs is approximately 1 day, [11], and 6-7 days, [10], for T_3 and T_4 , respectively. Therefore, TRH, TSH and THs have the fastest, intermediate and slowest dynamic behaviour, respectively, and hence, the geometric singular perturbation technique which has been widely used to analyze the system with different speeds of dynamic behaviours, [12], [13], [14], [15], [16], can be applied to analyze the system theoretically. By scaling the variables and parameters of the system by small positive values ε and δ as follows:

$$x = \frac{X}{X^*}, y = \frac{Y}{Y^*}, z = \frac{Z}{Z^*}, t = \frac{T}{T^*}, c_1 = \frac{T^* a_1}{(X^*)^2}, c_2 = T^* a_2,$$

$$c_3 = \frac{T^*}{\varepsilon Z^* (Y^*)^2}, c_4 = a_4, c_5 = Y^* a_5, c_6 = \frac{T^* a_6}{\varepsilon},$$

$$c_7 = \frac{T^* a_7}{\varepsilon \delta (Z^*)^2}, c_8 = \frac{T^* Y^* a_8}{\varepsilon \delta Z^*}, k_1 = \frac{h_1}{X^*}, k_2 = \frac{h_2}{Z^*}, k_3 = \frac{h_3}{X^*},$$

$$k_4 = \frac{h_4}{Z^*}, k_5 = \frac{h_5}{(Y^*)^2}, k_6 = \frac{h_6}{Z^*}, d_1 = T^*b_1, d_2 = \frac{T^*b_2}{\varepsilon},$$

$$d_3 = \frac{T^*b_3}{\varepsilon\delta}, \text{ the system of equations (1)-(3) becomes}$$

$$\frac{dx}{dt} = \frac{c_1}{k_1+x} + \frac{c_2xz}{k_2+z^2} - d_1x \equiv I(x, y, z) \quad (4)$$

$$\frac{dy}{dt} = \varepsilon \left[\frac{c_3xy(c_4+c_5y)}{(k_3+x)(k_4+z)(k_5+y^2)} - c_6y - d_2y \right]$$

$$\equiv \varepsilon J(x, y, z) \quad (5)$$

$$\frac{dz}{dt} = \varepsilon\delta \left[\frac{c_7}{k_6+z} + c_8y - d_3z \right] \equiv \varepsilon\delta K(x, y, z) \quad (6)$$

This means that x possesses the fastest dynamics, y possesses the intermediate dynamics and z possesses the slowest dynamics. Next, let us investigate the manifold $\{I=0\}$, $\{J=0\}$ and $\{K=0\}$ in detail.

The manifold $\{I=0\}$

By setting equation (4) equals to zero, we obtain

$$\frac{c_1}{(k_1+x)x} = d_1 - \frac{c_2z}{k_2+z^2}$$

Note that this equation does not depend on y and hence, the manifold $\{I=0\}$ is parallel to the y -axis.

The intersection of the manifold $\{I=0\}$ and the x -axis on the (x,z) -plane occurs at the point for which

$$x = \frac{-d_1k_1 + \sqrt{(d_1k_1)^2 + 4c_1d_1}}{2d_1} \equiv x_1 > 0 \text{ and } z = 0.$$

It also attains the relative maximum along the line

$$\{x = x_M, z = z_M\}$$

where

$$x_M \equiv \frac{-A_1k_1 \pm \sqrt{(A_1k_1)^2 + 4A_1c_1}}{2A_1}, A_1 \equiv d_1 - \frac{c_2\sqrt{k_2}}{2k_2}$$

and $z_M \equiv \sqrt{k_2}$. Note that $x_M > 0$ if and only if $A_1 > 0$, that is

$$d_1 > \frac{c_2\sqrt{k_2}}{2k_2} \quad (7)$$

The manifold $\{J=0\}$

By setting equation (5) equals to zero, we obtain $y=0$ and

$$z = \frac{1}{c_6+d_2} \left[\frac{c_3x(c_4+c_5y)}{(k_3+x)(k_5+y^2)} - k_4(c_6+d_2) \right] \equiv r(x, y)$$

Therefore, the manifold $\{J=0\}$ consists of two parts. The nontrivial manifold $z=r(x, y)$ intersects the trivial manifold $y=0$ along the curve that is asymptotic to the line $z=z_1$ where

$$z_1 \equiv \frac{c_3c_4 - k_4k_5(c_6+d_2)}{k_5(c_6+d_2)}.$$

Note that $z_1 > 0$ if

$$c_3c_4 > k_4k_5(c_6+d_2) \quad (8)$$

Moreover, on the (x,z) -plane, the nontrivial manifold $z=r(x, y)$ intersects the x -axis at the point for which $x=x_2$ and $z=0$ where

$$x_2 \equiv \frac{k_3k_4k_5(c_6+d_2)}{c_3c_4 - k_4k_5(c_6+d_2)}$$

Note that $x_2 > 0$ if the inequality (8) holds. In addition, the intersection of the nontrivial manifold $z=r(x, y)$ and the (x,y) -plane occurs along the curve

$$x = \frac{k_3k_4(c_6+d_2)(k_5+y^2)}{c_3(c_4+c_5y) - k_4(c_6+d_2)(k_5+y^2)} \equiv w(y)$$

$w(y)$ has a relative minimum at the point for which

$$y = y_m \equiv \frac{-c_4 + \sqrt{c_4^2 + c_5^2k_5}}{c_5} > 0$$

and $x = x_m \equiv \frac{k_3k_4(c_6+d_2)(k_5+y_m^2)}{c_3(c_4+c_5y_m) - k_4(c_6+d_2)(k_5+y_m^2)}.$

Since

$$\frac{\partial r}{\partial y} = \frac{c_3x}{(c_6+d_2)(k_3+x)} \left(\frac{-c_5y^2 - 2c_4y + c_5k_5}{(k_5+y^2)^2} \right)$$

then, $\frac{\partial r}{\partial y} = 0$ at the point where $y = y_m$. Moreover,

$$\left. \frac{\partial^2 r}{\partial y^2} \right|_{y=y_m} = \frac{c_3x}{(c_6+d_2)(k_3+x)} \left(\frac{-2c_5y_m - 2c_4}{(k_5+y_m^2)^2} \right) < 0$$

whenever $x > 0$. Therefore, the nontrivial manifold $z = r(x, y)$ obtains its relative maximum at the points for which $x = \alpha, y = y_m$ and

$$z = z_m = \frac{1}{(c_6 + d_2)} \left[\frac{c_3 \alpha (c_4 + c_5 y_m)}{(k_3 + \alpha)(k_5 + y_m^2)} - k_4 (c_6 + d_2) \right]$$

while α is any positive constant.

The manifold $\{K = 0\}$

By setting equation (6) equals to zero, we obtain

$$y = \frac{d_3 z^2 + d_3 k_6 z - c_7}{c_8 z + c_8 k_6} \equiv v(z) \quad (9)$$

We can see that this equation does not depend on x and hence, the manifold $y = v(z)$ is parallel to the x -axis. In addition, $y = v(z)$ intersects the z -axis at the point for which $y = 0$, and $z = z_2$ where

$$z_2 \equiv \frac{-d_3 k_6 + \sqrt{(d_3 k_6)^2 + 4c_7 d_3}}{2d_3} > 0$$

Moreover,

$$v'(z) = \frac{c_8 d_3 z^2 + 2c_8 d_3 k_6 z + c_7 c_8 + c_8 d_3 k_6^2}{(c_8 z + c_8 k_6)^2} > 0$$

whenever $z > 0$ and hence $v(z)$ is an increasing function and has no relative maximum or relative minimum for $z > 0$.

The different dynamic behaviours of solutions of the system of equations (4)-(6) could be expected when the locations of the manifolds $\{I = 0\}, \{J = 0\}$ and $\{K = 0\}$ are different.

Theorem 1 For sufficiently small ε and δ , suppose that

$$x_2 < x_1, \quad (10)$$

$$y_s < y_m, \quad (11)$$

$$z_2 < z_1 \quad (12)$$

and the inequality (8) holds then a limit cycle exists and a periodic solution occurs for the system of equations (4)-(6).

Given that the inequalities (8) and (10)-(12) identified in Theorem 1 are satisfied, the manifolds $\{I = 0\}, \{J = 0\}, \{K = 0\}$ will be positioned as shown in Figure 1 (Appendix). Starting from the point O as located in Figure 1 (Appendix), a transition in the direction of decreasing x with the fast speed, since $I < 0$ here, will bring the solution trajectory to the fast manifold $\{I = 0\}$ where a point

P is reached. Since $J < 0$ here, an intermediate transition develops along the manifold $\{I = 0\}$ in the direction of decreasing y until the point Q on the stable branch of $\{I = J = 0\}$ is reached. A transition in the direction of decreasing z at a slow speed then develops along $\{I = J = 0\}$ until it reaches the point R for which the manifold loses its stability. A jump with an intermediate speed in the direction of increasing y from the point R will then bring the solution trajectory to the other stable branch of $\{I = J = 0\}$ where the point T is reached. A slow transition will develop in the direction of increasing z , since $K > 0$ here, from the point T to the point U. A transition of the solution trajectory then brings the system to the other stable branch of $\{I = J = 0\}$ where the point V is reached. This is followed by a slow transition which brings the system from the point V to the point R resulting in a closed cycle RTUV and hence, the system of equations (4) - (6) exhibits a limit cycle and a periodic solution then occurs.

Theorem 2 For sufficiently small ε and δ , suppose that

$$x_1 < x_4 < x_m, \quad (13)$$

then the steady state $S_1 = (x_4, 0, z_2)$ of the system of equations (4)-(6) is stable.

Given that the inequality (13) identified in Theorem 2 are satisfied, the manifolds $\{I = 0\}, \{J = 0\}, \{K = 0\}$ will be positioned as shown in Figure 2 (Appendix). In Figure 2 (Appendix), starting from the in front of the manifold $\{I = 0\}$ at a point O which is above the manifold $\{J = 0\}$. A fast transition in the direction of decreasing x will bring the solution trajectory to a point P on the fast manifold $\{I = 0\}$ since $I < 0$ here. Since $J < 0$ here, the transition in the direction of decreasing y at intermediate speed develops along the manifold $\{I = 0\}$ until it reaches the point Q on stable branch of $\{I = J = 0\}$. Here $K < 0$, a transition at a slow speed in the direction of decreasing z then develops along this curve until it reaches the equilibrium point $S_1 = (x_4, 0, z_2)$ where $I = J = K = 0$.

Therefore, the washout equilibrium point $S_1 = (x_4, 0, z_2)$ is stable in this case and the solution trajectory tends toward S_1 as time passes.

Theorem 3 For sufficiently small ε and δ , suppose that

$$x_2 < x_1 \quad (14)$$

$$y_m < y_s, \quad (15)$$

and the inequality (8) holds then the system of equations (4)-(6) has a stable steady state $S_2 = (x_s, y_s, z_s)$.

Given that the inequalities (8), (14)-(15) identified in Theorem 3 are satisfied, the manifolds $\{I=0\}, \{J=0\}, \{K=0\}$ will be positioned as shown in Figure 3 (Appendix). In Figure 3 (Appendix), starting from the in front of the manifold $\{I=0\}$ at a point O which is above the manifold $\{J=0\}$. A fast transition in the direction of decreasing x will bring the solution trajectory to a point P on the fast manifold $\{I=0\}$ since $I < 0$ here. A transition in the direction of decreasing y at intermediate speed develops along the manifold $\{I=0\}$ to the point Q on stable branch of $\{I=J=0\}$. A transition at a slow speed in the direction of decreasing z then brings the solution trajectory to point R in which the stability of the manifold is lost. A jump in the direction of increasing y at intermediate speed will then bring the system to the point T on the other stable branch of $\{I=J=0\}$. since $K > 0$ here, a transition in the direction of increasing z at slow speed then brings the solution trajectory to the point $S_2 = (x_s, y_s, z_s)$ where $I = J = K = 0$. Therefore, the equilibrium point $S_2 = (x_s, y_s, z_s)$ is stable and the solution trajectory tends toward S_2 as time passes.

3 Numerical Simulations

In this section, we illustrate the theoretical results by carrying out numerical simulations for each case. All simulations are generated by MATLAB using the Runge-Kutta 4th-order method.

The computer simulation shown in Figure 4 (Appendix) is presented to illustrate the theoretical prediction in Theorem 1 in which a limit cycle is

expected provided that the inequalities stated in Theorem 1 are all satisfied.

We can see that the solution of the system of equations (4)-(6) shown in Figure 4 (Appendix) tends toward a limit cycle and a periodic solution occurs as theoretically predicted in Theorem 1.

The computer simulation shown in Figure 5 (Appendix) is presented to illustrate the theoretical prediction in Theorem 2 in which the equilibrium point S_1 is stable provided that the inequality stated in Theorem 2 is satisfied.

We can see that the solution of the system of equations (4)-(6) shown in Figure 5 (Appendix) tends toward the equilibrium point S_1 as theoretically predicted in Theorem 2.

The computer simulation shown in Figure 6 (Appendix) is presented to illustrate the theoretical prediction in Theorem 3 in which the equilibrium point S_2 is stable provided that the inequalities stated in Theorem 3 are all satisfied.

We can see that the solution of the system of equations (4)-(6) shown in Figure 6 (Appendix) tends toward the equilibrium point S_2 as theoretically predicted in Theorem 3.

4 Discussion and Conclusion

We develop a mathematical model to investigate the effect of exposure to PFOS/PFOA on thyroid homeostasis. Theoretically, the geometric singular perturbation technique is utilized so that we obtain the conditions on the system parameters that differentiate various behaviours of the solutions of our model. Numerical simulations are provided to illustrate the theoretical results. Both theoretical and numerical results indicate that a periodic behaviour that has been observed in the pulsatile secretions of TRH, TSH and THs, [17], [18], [19], could be exhibited by our model when the parametric values are appropriated. In addition, let us consider an example of the computer simulations in Figure 7 (Appendix) for the case when there is no effect of PFOS/PFOA ($c_6 = 0$) and the case when

there is the effect of PFOS/PFOA ($c_6 = 0.08$) while the other parametric values are the same that is $c_1 = 0.15, c_2 = 0.30,$

$c_3 = 0.55, c_4 = 0.80, c_5 = 0.7, c_7 = 0.21, c_8 = 0.7, k_1 = 0.95,$
 $k_2 = 0.75, k_3 = 0.9, k_4 = 0.5, k_5 = 0.3, k_6 = 0.7, d_1 = 0.55,$
 $d_2 = 0.1, d_3 = 0.03, \varepsilon = 0.95, \delta = 0.035$ with
 $x(0) = 0.1, y(0) = 0.5,$ and $z(0) = 2$. We can see

that when there is the effect of PFOS/PFOA, the levels of TSH and THs are lower than those of the case when there is no effect of PFOS/PFOA which might lead to the imbalance of thyroid homeostasis and hence, the hypothyroidism might be expected. The developed model might be useful to investigate further the treatment of hypothyroidism due to exposure to PFOS and PFOA.

Acknowledgement:

This work is supported by the Centre of Excellence in Mathematics, Thailand and Mahidol University, Thailand.

References:

- [1] Leko, M. B., Gunjaca, I., Pleic, N., Zemunik, T. Environmental factors affecting thyroid-stimulating hormone and thyroid hormone levels. *Int. J. Mol. Sci.*, 2021. 22: 6521. <https://doi.org/10.3390/ijms22126521>
- [2] Dietrich, J.W., Landgrafe, G., Fotiadou, E.H. TSH and thyrotropic agonists: key actors in thyroid homeostasis. *J. Thyroid Res.*, 2012. 2012: 351864. doi: 10.1155/2012/351864
- [3] Coperchini, F., Croce, L., Ricci, G., Magri, F., Rotondi, M., Imbriani, M., Chiovato, L. Thyroid disrupting effects of old and new generation PFAS. *Front. Endocrinol.*, 2021. 11: 612320. doi: 10.3389/fendo.2020.612320
- [4] Buck, R.C., Franklin, J., Berger, U., Conder, J.M., Cousins, I.T., De Voogt, P., Jensen, A.A., Kannan, K., Mabury, S.A., van Leeuwen, S.P.J. Perfluoroalkyl and polyfluoroalkyl substances in the environment: Terminology, classification, and origins. *Integr. Environ. Assess. Manag.*, 2011. 7: 513–541, doi:10.1002/ieam.258.
- [5] Jian, J.M., Chen, D., Han, F.J., Guo, Y., Zeng, L., Lu, X., et al. A short review on human exposure to and tissue distribution of per- and polyfluoroalkyl substances (PFASs). *Sci. Total Environ.*, 2018. 636:1058–69. doi: 10.1016/j.scitotenv.2018.04.380.
- [6] Stableski, J., Salihovic, S., Lind, L., Lind, P.M., van Bavel, B., Kärrman, A. Changes in serum levels of perfluoroalkyl substances during a 10-year follow-up period in a large population-based cohort. *Environ. Int.*, 2016. 95:86–92. doi: 10.1016/j.envint.2016. 08.002
- [7] Hong, S., Khim, J.S., Park, J., Kim, M., Kim, W.K., Jung, J., et al. In situ fate and partitioning of waterborne perfluoroalkyl acids (PFAAs) in the Youngsan and Nakdong River Estuaries of South Korea. *Sci. Total Environ.*, 2013. 445-446:136–45. doi: 10.1016/j.scitotenv.2012.12. 040
- [8] Coperchini, F., Awwad, O., Rotondi, M., Santini, F., Imbriani, M., Chiovato, L. Thyroid disruption by perfluorooctane sulfonate (PFOS) and perfluorooctanoate (PFOA). *J. Endocrinol. Invest.*, 2017. 40:105-121.
- [9] Duntas, L., Keck, F.S., Rosenthal, J., Wolf, C.H., Loos, U., Pfeiffer, E.F., Wochenshrift, K. Single-compartment model analysis of thyrotropin-releasing hormone kinetics in hyper- and hypothyroid patients. *Klin. Wochenschr.*, 1990. 68:1013-1019.
- [10] Barrett, K., Brooks, H., Boitano, H., Barman, S. *The Thyroid Gland. Review of Medical Physiology*, 23rd ed., The McGraw-Hill Companies, Inc., 2010. 305-307.
- [11] Jonklaas, J., Burman, K.D., Wang, H., Latham, K.R. Single dose T3 administration: kinetics and effects on biochemical and physiologic parameters. *Ther. Drug. Monit.*, 2015. 37(1): 110-118.
- [12] Muratori, S., Rinaldi, S. Low-and high-frequency oscillations in three dimensional food chain systems. *Siam J. Appl. Math.*, 1992. 52:1688-1706.
- [13] Manorod, S., Rattanaku, C. Modelling the population dynamics of brown planthopper, *Cyrtorhinus lividipennis* and *Lycosa pseudoannulata*. *Advances in Difference Equations*, 2019. 2019:265. doi: 10.1186/s13662-019-2217-y
- [14] Rattanaku, C., Lenbury, Y., Krishnamara, N., Wollkind, D.J. Mathematical modelling of bone formation and resorption mediated by parathyroid hormone: Responses to estrogen/PTH therapy. *BioSystems.*, 2003. 70: 55-72.
- [15] Lenbury, Y., Ruktamatakul, S., Amornsamankul, S. Modeling insulin kinetics: responses to a single oral glucose administration or ambulatory-fed conditions. *BioSystems*, 2001. 59:15-25.
- [16] Rattanaku, C., Rattanamongkonkul, S. Effect of Calcitonin on Bone Formation and Resorption: Mathematical Modeling Approach. *Int. J. Mathl. Mod. Meth. Appl. Sci.*, 2011. 5(8):1363-1371.
- [17] Villares, S., Knoepfelmacher, M., Salgado, L. et al. Pulsatile Release and Circadian Rhythms of Thyrotropin and Prolactin in Children with

Growth Hormone Deficiency. *Pediatr. Res.*, 1996. 39:1006–1011.

- [18] Roelfsema, F., Veldhuis, J.D. Thyrotropin Secretion Patterns in Health and Disease. *Endocrine Reviews*, 2013. 34(5):619–657.
- [19] Brabant, G., Prank, K., Ranft, U., Schuermeyer, T.H., Wagner, T.O.F., Hauser, H., Kummer, B., Feistner, H., Hesch, R.D., MüHlen, A.V.Z. Physiological Regulation of Circadian and Pulsatile Thyrotropin Secretion in Normal Man and Woman. *The Journal of Clinical Endocrinology & Metabolism*, 1990. 70(2):403–409.

Appendix

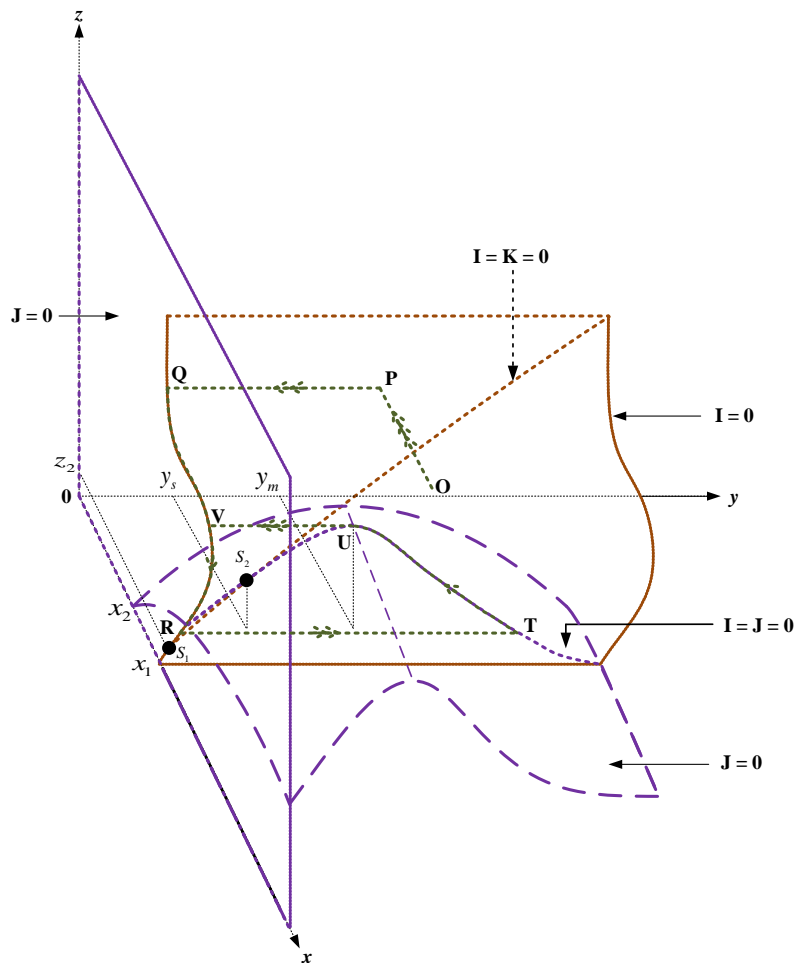


Fig. 1: The positions of the manifolds $\{I=0\}, \{J=0\}$ and $\{K=0\}$ where all inequalities stated in Theorem 1 are satisfied. A solution trajectory tends toward a limit cycle where the fast, intermediate and slow transitions are identified by the three, two and one arrows, respectively.

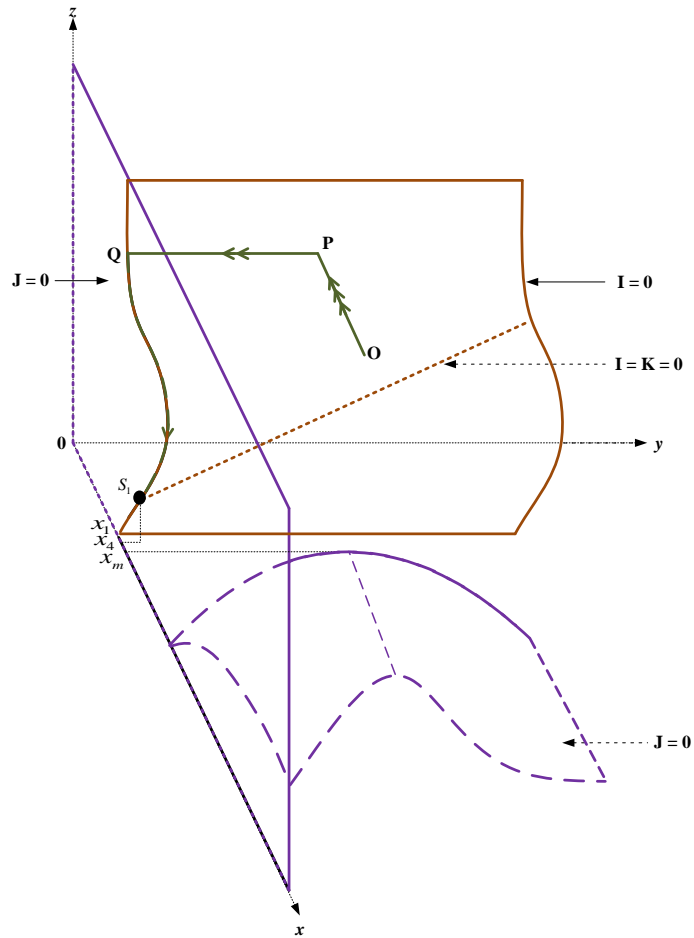


Fig. 2: The positions of the manifolds $\{I=0\}$, $\{J=0\}$ and $\{K=0\}$ where the inequality stated in Theorem 2 are satisfied. A solution trajectory tends toward a stable equilibrium point S_1 where the fast, intermediate and slow transitions are identified by the three, two and one arrows, respectively.

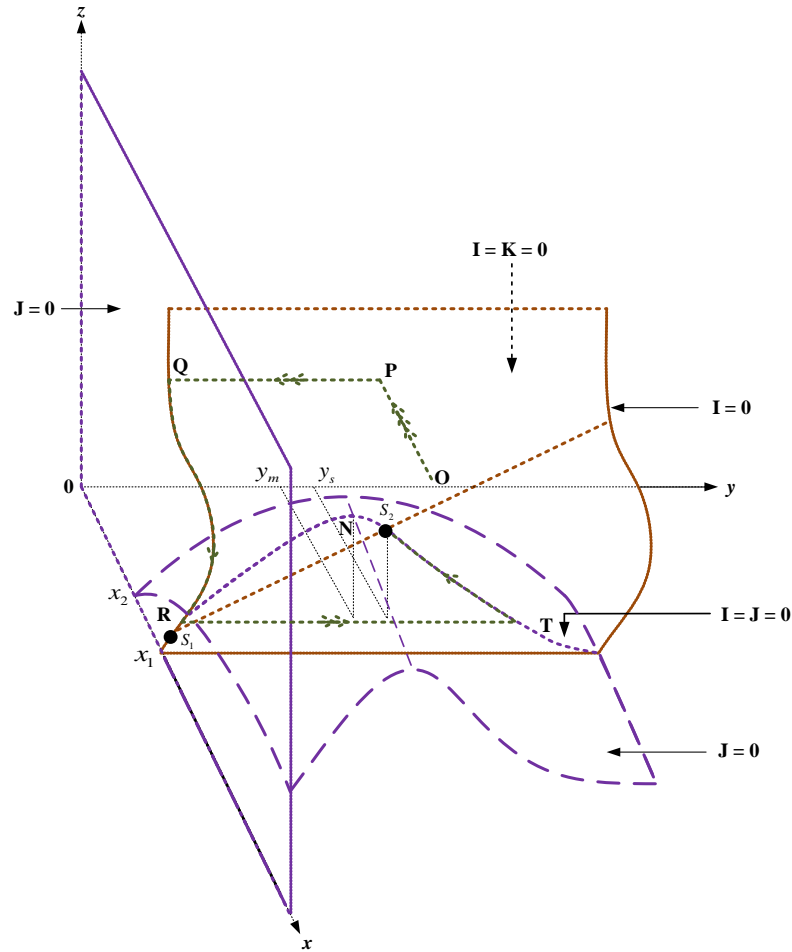


Fig. 3: The positions of the manifolds $\{I=0\}, \{J=0\}$ and $\{K=0\}$ where all inequalities stated in Theorem 3 are satisfied. A solution trajectory tends toward a stable equilibrium point S_2 where the fast, intermediate and slow transitions are identified by the three, two and one arrows, respectively.

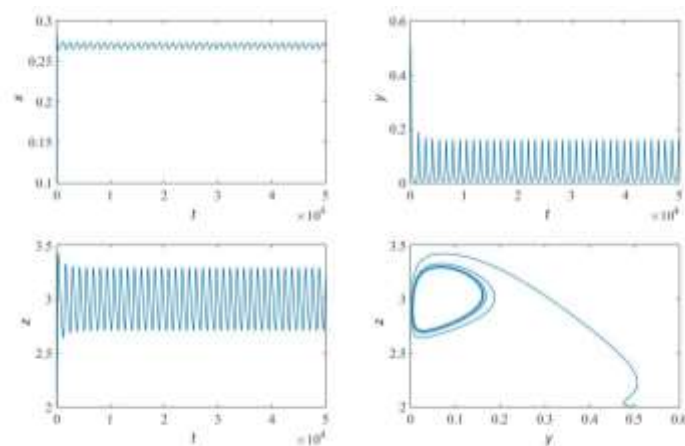


Fig. 4: A simulation result of the system of equations (4)-(6) where $c_1 = 0.15, c_2 = 0.30, c_3 = 0.55, c_4 = 0.80, c_5 = 0.70, c_6 = 0.08, c_7 = 0.21, c_8 = 0.7, k_1 = 0.95, k_2 = 0.75, k_3 = 0.90, k_4 = 0.50, k_5 = 0.30, k_6 = 0.70, d_1 = 0.55, d_2 = 0.02, d_3 = 0.03, \varepsilon = 0.95, \delta = 0.035, x(0) = 0.1, y(0) = 0.5,$ and $z(0) = 2.$

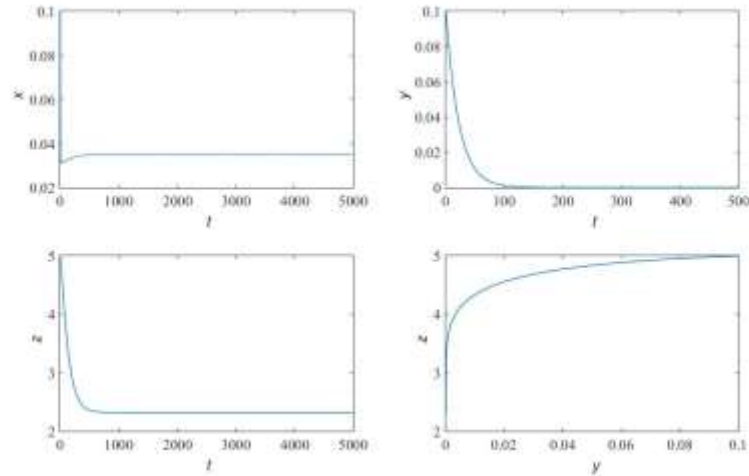


Fig. 5: A simulation result of the system of equations (4)-(6) where $c_1 = 0.015, c_2 = 0.3, c_3 = 0.55, c_4 = 0.8, c_5 = 0.7, c_6 = 0.08, c_7 = 0.21, c_8 = 0.7, k_1 = 0.95, k_2 = 0.75, k_3 = 0.9, k_4 = 0.5, k_5 = 0.3, k_6 = 0.7, d_1 = 0.55, d_2 = 0.02, d_3 = 0.03, \varepsilon = 0.5, \delta = 0.35, x(0) = 0.1, y(0) = 0.1,$ and $z(0) = 5$.

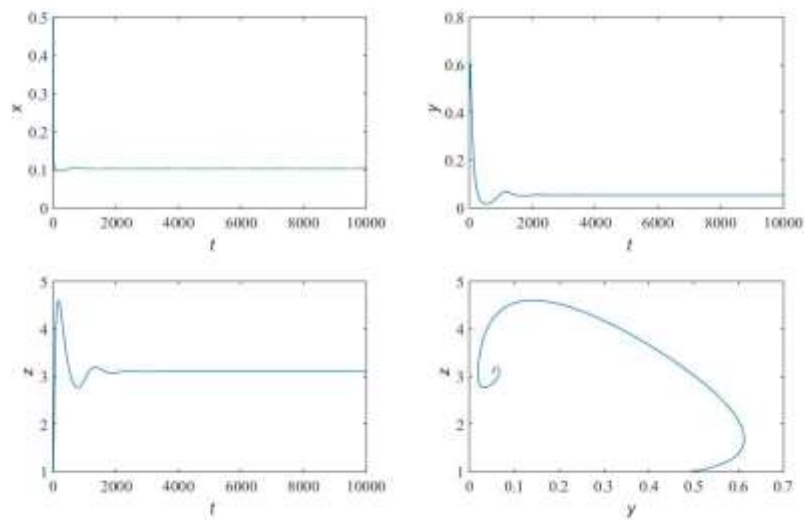


Fig. 6: A simulation result of the system of equations (4)-(6) where $c_1 = 0.05, c_2 = 0.30, c_3 = 0.55, c_4 = 0.80, c_5 = 0.4, c_6 = 0.1, c_7 = 0.21, c_8 = 0.7, k_1 = 0.95, k_2 = 0.75, k_3 = 0.10, k_4 = 0.5, k_5 = 0.3, k_6 = 0.7, d_1 = 0.55, d_2 = 0.11, d_3 = 0.03, \varepsilon = 0.15, \delta = 0.75, x(0) = 0.5, y(0) = 0.5,$ and $z(0) = 1$.

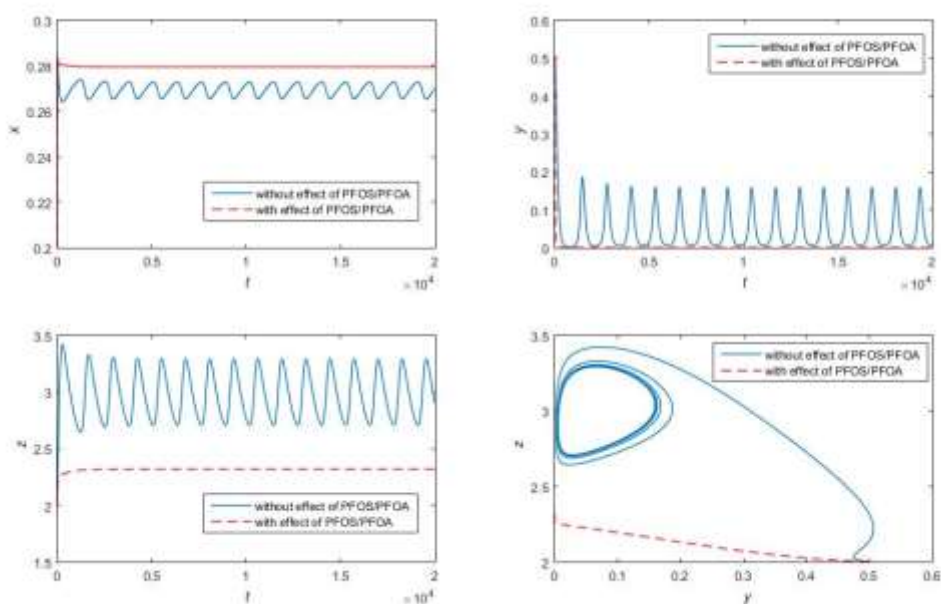


Fig. 7: Comparison of the simulation results of the system of equations (4)-(6) for the case $c_6 = 0$ (without the effect of PFOS/PFOA) and $c_6 = 0.08$ (with the effect of PFOS/PFOA). Here, $c_1 = 0.15, c_2 = 0.30, c_3 = 0.55, c_4 = 0.80, c_5 = 0.7, c_7 = 0.21, c_8 = 0.7, k_1 = 0.95, k_2 = 0.75, k_3 = 0.9, k_4 = 0.5, k_5 = 0.3, k_6 = 0.7, d_1 = 0.55, d_2 = 0.1, d_3 = 0.03, \varepsilon = 0.95, \delta = 0.035, x(0) = 0.1, y(0) = 0.5,$ and $z(0) = 2$.

Contribution of Individual Authors to the Creation of a Scientific Article (Ghostwriting Policy)

The author contributed to the present research at all stages including the formulation of the problem, the theoretical analysis of the model, numerical investigations as well as preparation of the manuscripts.

Sources of Funding for Research Presented in a Scientific Article or Scientific Article Itself

This work is supported by the Centre of Excellence in Mathematics, Thailand and Mahidol University, Thailand.

Conflict of Interest

The author has no conflicts of interest to declare that are relevant to the content of this article.

Creative Commons Attribution License 4.0 (Attribution 4.0 International, CC BY 4.0)

This article is published under the terms of the Creative Commons Attribution License 4.0

https://creativecommons.org/licenses/by/4.0/deed.en_US